Letter

Surface termination conversion effect on the electronic structure of two-dimensional electron gas at $EuTiO_3$ surfaces

Sungsoo Hahn,[1,2] Keun-Yeol Park,[1] Minkyu Park,[2] Yeonjae Lee,[1] Youngdo Kim,[1] S. H. Rhim,[3] Celesta S. Chang,[1] Chanyong Hwang,[2] and Changyoung Kim[1,*]

[1]*Department of Physics and Astronomy, Seoul National University, Seoul 08826, Korea*

[2]*Quantum Technology Institute, Korea Research Institute of Standards and Science (KRISS), Daejeon 34113, Republic of Korea*

[3]*Department of Semiconductor Physics and Engineering, University of Ulsan, Ulsan 44610, Korea*

(Received 31 July 2025; accepted 23 January 2026; published 11 February 2026)

We perform *in situ* angle-resolved photoemission spectroscopy to investigate the effect of surface termination conversion on two-dimensional electron gas (2DEG) at the $EuTiO_3$(001) surface. We successfully engineered $EuTiO_3$ with nearly single TiO_2 termination via epitaxial growth on TiO_2-terminated $SrTiO_3$, and $EuTiO_3$ with nearly complete EuO termination by inserting a $SrRuO_3$ buffer layer into the heterostructure. The orbital configuration of the 2DEG exhibits a strong dependence on the $EuTiO_3$ termination, and this experimental observation matches our first-principles calculation results very well. Furthermore, we observe the termination dependence of a kink feature in d_{xy} band. This finding implies that many-body interactions, and possibly magnetism, are influenced by the surface termination. Our study not only introduces a method to fabricate surface or interfacial 2DEG system, but also highlights the effect of termination conversion on magnetic 2DEG.

DOI: 10.1103/dx5k-dwgv

Surface and interfacial systems have drawn significant attention due to their potential to host novel physical phenomena, arising from broken inversion symmetry and their two-dimensional nature [1–3]. Two-dimensional electron gas (2DEG) systems at the surfaces or interfaces of insulating oxides are of particular interest [4–6]. Various novel phenomena—such as the quantum Hall effect [7], two-dimensional superconductivity [8,9], magnetism [10,11], the coexistence of magnetism and superconductivity [12–14], and tunable spin-orbit coupling [15–18]—have been experimentally realized in 2DEG systems. Notably, all the aforementioned phenomena can be realized by employing appropriate materials or engineering the necessary surface or interface configurations. These degrees of freedom make 2DEG systems a promising platform for discovering new physical phenomena. Consequently, a wide range of heterostructures and interfaces are being actively investigated [19–25].

Among the various interfaces, magnetic interface is of particular interest due to their potential for spintronic application as well as novel phenomena [26–30]. One of the promising materials for magnetic 2DEG systems is $EuTiO_3$ (ETO), an insulating compound with a perovskite structure. Similar to the extensively studied $SrTiO_3$ (STO) [5], the bands near the Fermi level (E_F) in ETO with hybridized Ti $3d$-O $2p$ character contribute to the formation of 2DEG [31–35]. Additionally, Eu^{2+} possess a magnetic moment close to the value of $7\mu_B$/Eu [36], owing to their localized $4f^7$ electrons. As a result, ETO exhibits a spin-polarized band approximately 2 eV below E_F [32]. This magnetic property sets ETO apart from STO and enables spin-related phenomena such as Weyl nodes, the anomalous Hall effect, and the topological Hall effect [37–40]. These characteristics highlight the rich potential of ETO-based interfaces and heterostructures. Therefore, it is crucial to manipulate these properties to harness the capabilities of ETO.

Surface termination conversion is an effective approach to tailoring interface or surface properties [41–45]. In particular, it has been reported that the electronic properties of various perovskie oxides can be tuned through surface termination conversion [46,47]. Therefore, preparing well-defined surfaces and achieving precise control over termination are of significant importance. In this study, we report the experimental realization of surface termination conversion in ETO using pulsed laser deposition (PLD) method. Our strategy is to insert a $SrRuO_3$ (SRO) buffer layer to exploit its A-site termination characteristics [48], allowing control over the termination of ETO surface. We further investigate the impact of this termination on the electronic structure of the 2DEG via *in situ* angle-resolved photoemission spectroscopy (ARPES) studies. Our ARPES results clearly reveal the evolution of orbital configuration in the 2DEG depending on the surface termination, consistent with density functional theory (DFT) calculations and with previous experimental and theoretical results [32]. Moreover, we find that surface termination also affects the kink structure in the 2DEG bands. Our experimental study demonstrates how the electronic structure of a magnetic 2DEG can be effectively modulated through surface termination engineering.

B-site(TiO_2)-terminated ETO thin films were grown on the B-site terminated and (001)-oriented STO substrates (Shinkosha) directly using PLD technique. For the growth of A-site (EuO)-terminated ETO, we used an SRO buffer layer

*Contact author: changyoung@snu.ac.kr

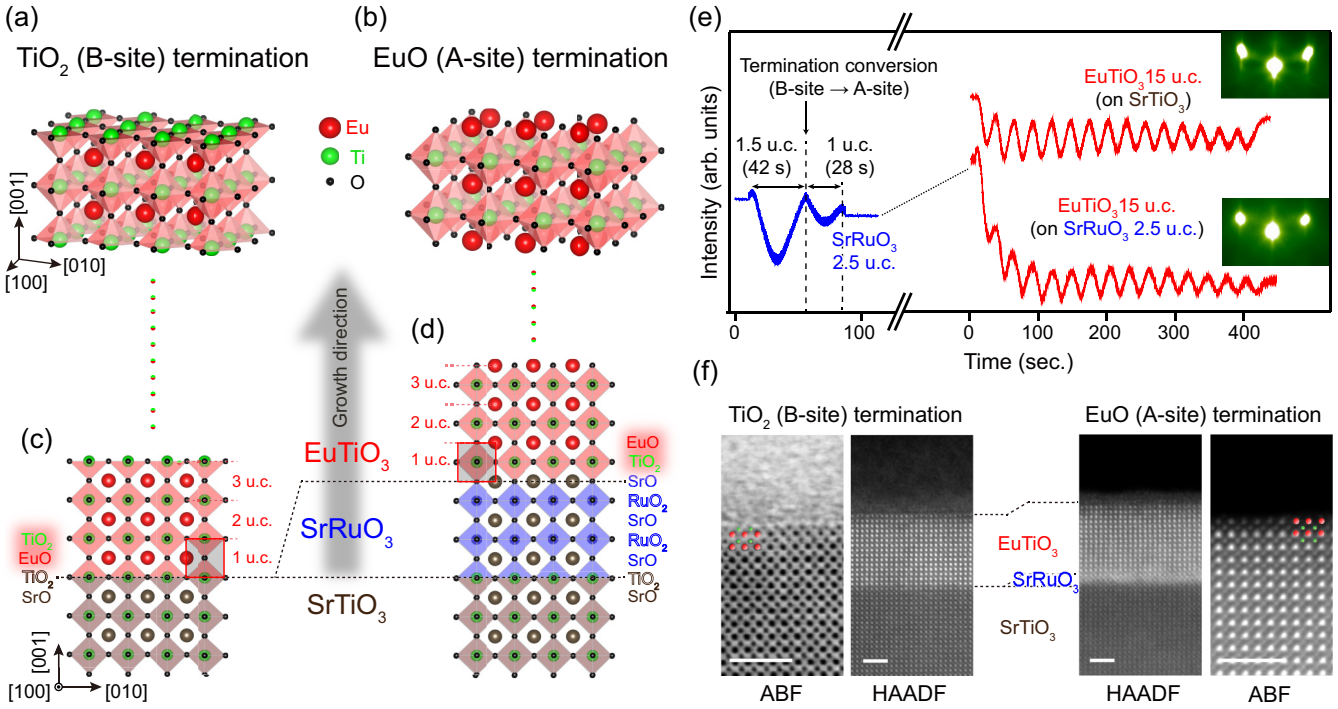

FIG. 1. Termination engineering in $EuTiO_3$ (ETO) heterostructure. Geometry of (a) TiO_2 (B-site)-terminated and (b) EuO(A-site)-terminated ETO film near the surface. Red, green, and black spheres represent Eu, Ti, and O atoms, respectively. Schematics of (c) ETO/$SrTiO_3$ (ETO/STO) and (d) ETO/$SrRuO_3$/STO (ETO/SRO/STO) heterostructure. ETO/STO (ETO/SRO/STO) heterostructure is terminated with TiO_2 (EuO) layer. Both heterostructures were grown on TiO_2(B-site)-terminated STO. (e) Reflection high-energy electron diffraction (RHEED) intensity oscillation during the heterostructure growth. RHEED images taken after the deposition of heterostructures followed by postannealing with each termination are included. (f) Cross-sectional scanning transmission electron microscopy (STEM) images of ETO heterostructures. The second and third images show high-angle annular dark-field (HAADF) STEM images of the 5 nm Se capped ETO/STO and ETO/SRO/STO heterostructures, respectively, illustrating the overall structure. For STEM measurement, we use ten unit cell ETO layer. The first and fourth images show magnified annular bright-field (ABF) STEM and HAADF STEM images revealing the TiO_2 and EuO terminations in each structure. The crystal structures of ETO are overlaid for a guide to the eye. All scale bars represent 2 nm.

between ETO and substrate. Stoichiometric polycrystalline SRO and polycrystalline $Eu_2Ti_2O_7$ targets were ablated using a KrF excimer laser ($\lambda = 248$ nm, Coherent). During the SRO (ETO) growth, the substrate temperature, background oxygen partial pressure, laser fluence, and repetition rate were kept at 670 °C (600 °C), 100 mTorr (10^{-7} mTorr), 1.9 J/cm^2 (0.8J/cm^2), and 2 Hz (1 Hz), respectively. The thickness of SRO and ETO were 2.5 and 15 unit cells (u.c.), respectively, to avoid unintentional ferromagnetic proximity effect from SRO layer to ETO surface. For the 15 u.c. ETO films, we observed no variation in the ARPES spectra, even when the thickness of the SRO buffer layer was increased up to 8 u.c., as shown in Fig. S1 of the Supplemental Material [49] (see also Ref. [50] therein). The growth dynamics were monitored by the reflection high-energy electron diffraction (RHEED) technique during the growth. To induce 2DEG at the surface, ETO film was postannealed at 600 °C under ultrahigh vacuum ($<1 \times 10^{-8}$ mTorr) conditions for 30 minutes after cooling the grown sample to 200 °C. *In situ* ARPES measurements were performed in a laboratory-based system equipped with a Scienta DA30 analyzer using He-Iα ($h\nu = 21.22$ eV) light at 10 K. The scanning transmission electron microscopy (STEM) lamella samples were prepared using an FEI Helios G4 focused ion beam (FIB) system. Rough milling was performed at an accelerating voltage of 30 kV with an ion beam current of 0.44 nA, followed by sequential low-energy thinning at 5 kV and 63 pA, and a final cleaning step at 2 kV and 66 pA to minimize surface damage. High-angle annular dark-field (HAADF) and annular bright-field (ADF) STEM images were obtained using a Thermo Fisher Scientific Themis Z aberration-corrected and monochromated microscope operated at 300 kV with a probe current of 90 pA and a dwell time of 2 μs. The collection angles were 21–126 mrad for HAADF and 6–13 mrad for ABF imaging. For the first-principles calculations, the Quantum ESPRESSO [51,52] package was used. Pseudopotentials were chosen from a standard solid-state pseudopotentials (SSSP) library [53–56] (SSSP PBEsol Precision v1.3.0). The calculations were performed for stoichiometric, antiferromagnetic, and insulating $EuTiO_3$ without including spin-orbit interactions. Hubbard U corrections [57] with $U = 7.5$ eV and $U = 2$ eV were applied for Eu and Ti, respectively [32]. The lattice constant was set to 3.905 Å [32] without performing structural relaxation. To investigate the effect of surface termination, we constructed a symmetric slab of ETO approximately 20 Å thick, with a vacuum region of at least 10 Å, for each termination.

The perovskite ETO consists of alternating layers of EuO and TiO_2 stacked along the pseudocubic [001] direction. There are two possible surface terminations for ETO, as

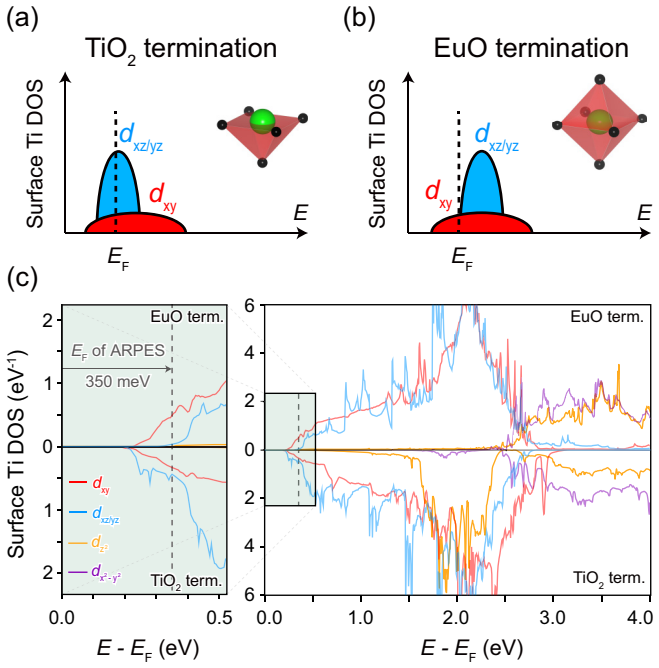

FIG. 2. Orbital configurations of the 2DEG depend on termination. Schematic orbital-resolved band structure diagrams of 2DEG at (a) TiO_2(B-site)-terminated and (b) EuO(A-site)-terminated surface. Structure of topmost TiO_6 octahedra, corresponding to each termination are shown. (c) Orbital-resolved density of states projected onto the top two ETO layers for each termination. The calculations were performed for stoichiometric, antiferromagnetic, and insulating ETO. To account for the electron doping required to form a 2DEG, the Fermi level was shifted by +350 meV, based on angle-resolved photoemission spectroscopy (ARPES) results discussed later.

illustrated in Figs. 1(a) and 1(b). The main difference between them lies in the structure of the topmost TiO_6 octahedron. In the case of the TiO_2-terminated surface shown in Fig. 1(a), the loss of the apex oxygen from the TiO_2 octahedron results in the exposure of Ti atoms at the surface. In contrast, for the EuO-terminated surface shown in Fig. 1(b), the topmost TiO_6 octahedra retain all their oxygen atoms and structural integrity. These structural differences affect the electrostatic potential experienced by the electrons, depending on their orbital components [47], as will be discussed later in Fig. 2(a).

Our strategy to control the termination relies on the fact that the termination of PLD-grown perovskite films, which depends on thickness and deposition conditions, tends to match that of the substrates [58]. For example, a mostly TiO_2- (EuO-)terminated ETO can be obtained by PLD deposition on a TiO_2-terminated (SrO-terminated) STO substrate. For example, an ETO film terminates with a TiO_2 (EuO) layer when deposited on a TiO_2-terminated (SrO-terminated) $SrTiO_3$ substrate. Accordingly, preparing substrates with well-defined and distinct terminations is a critical step. We achieve this by inserting a SRO buffer layer as a "termination conversion layer." SRO is one of the exceptional perovskite materials that terminates at the A site, even when grown on a B-site-terminated substrate. This surface conversion occurs when the transition metal at the perovskite B site is volatile, an effect reported in SRO [48] and $SrIrO_3$ [59]. Leveraging this unique growth behavior of SRO, we prepare an A-site-terminated SRO/STO heterostructure as a substrate to deposit an A-site-terminated ETO film, corresponding to the EuO-terminated ETO shown in Figs. 1(c) and 1(d).

We have experimentally verified that our growth method indeed modulates the termination of the film. As shown in Fig. 1(e), we experimentally confirmed a 1.5-fold difference in the time required for the deposition of the first SRO layer compared to the second layer. Furthermore, the ETO growth rate remained identical whether the SRO buffer layer was present or not, and this rate was consistently maintained during the ETO deposition process. Based on these kinetic observations, we could anticipate that the topmost layers of the ETO/STO and ETO/SRO/STO heterostructures are well defined with TiO_2- and EuO-termination, respectively. To confirm this prediction more definitively, we performed STEM experiments, which allow for direct visualization of the atomic termination. The STEM image in Fig. 1(f) clearly shows that the topmost layer of the ETO/STO structure is TiO_2 terminated, highlighted by the green spheres corresponding to the Ti atoms. Conversely, the topmost layer of the ETO/SRO/STO structure is mostly EuO terminated, highlighted by the red spheres corresponding to the Eu atoms. This STEM image provides direct experimental evidence that each heterostructure possesses the anticipated termination.

Figures 2(a) and 2(b) schematically show the structure of the topmost TiO_6 octahedron and their corresponding electronic structures. Assuming electron doping induced by oxygen vacancies, three Ti 3d t_{2g} bands (d_{xy}, d_{xz}, and d_{yz}) that contribute to the 2DEG are located near E_F. The energy hierarchy of these t_{2g} bands is rearranged by the surface termination.

At the TiO_2-terminated surface, absence of the apex oxygen lowers the energy of the out-of-plane oriented $d_{xz/yz}$ bands relative to the in-plane d_{xy} band. Confinement and structural surface relaxation lower the energy of the d_{xy} band with respect to the $d_{xz/yz}$ bands, similar to what is observed for STO surfaces. At the EuO-terminated surface, however, the TiO_6 octahedra at the topmost layer remain structurally intact, resulting in a uniform distribution of oxygen atoms in all directions. Accordingly, $d_{xz/yz}$ bands are pushed above E_F, d_{xy} bands further lower their energy, and energy splitting between d_{xy} and $d_{xz/yz}$ bands increases.

To confirm this termination-dependent behavior of the t_{2g} bands, we performed DFT calculations of slab structures for each termination. Figure 2(c) shows the orbital-resolved density of states (DOS) projected onto the top two ETO layers. By comparing the upper panel (EuO termination) and the lower panel (TiO_2 termination), we clearly observe the energy differences among the d orbitals. As expected, in the case of EuO termination, the energies of the $d_{xz/yz}$ (and d_{z^2}) bands are higher, while the energies of the d_{xy} (and $d_{x^2-y^2}$) bands are lower compared to the TiO_2-terminated case.

To verify the computational results, we performed *in situ* ARPES measurements. The observed termination-dependent electronic structures are shown alongside the corresponding DFT calculations for comparison. The DFT results were rigidly shifted by +350 meV from the E_F of stoichiometric ETO to align with the ARPES data. For the TiO_2-terminated ETO, ARPES reveals three bands, which are assigned to the d_{xz} (green), d_{yz} (blue), and (2 × 2) folded d_{xy} (red).

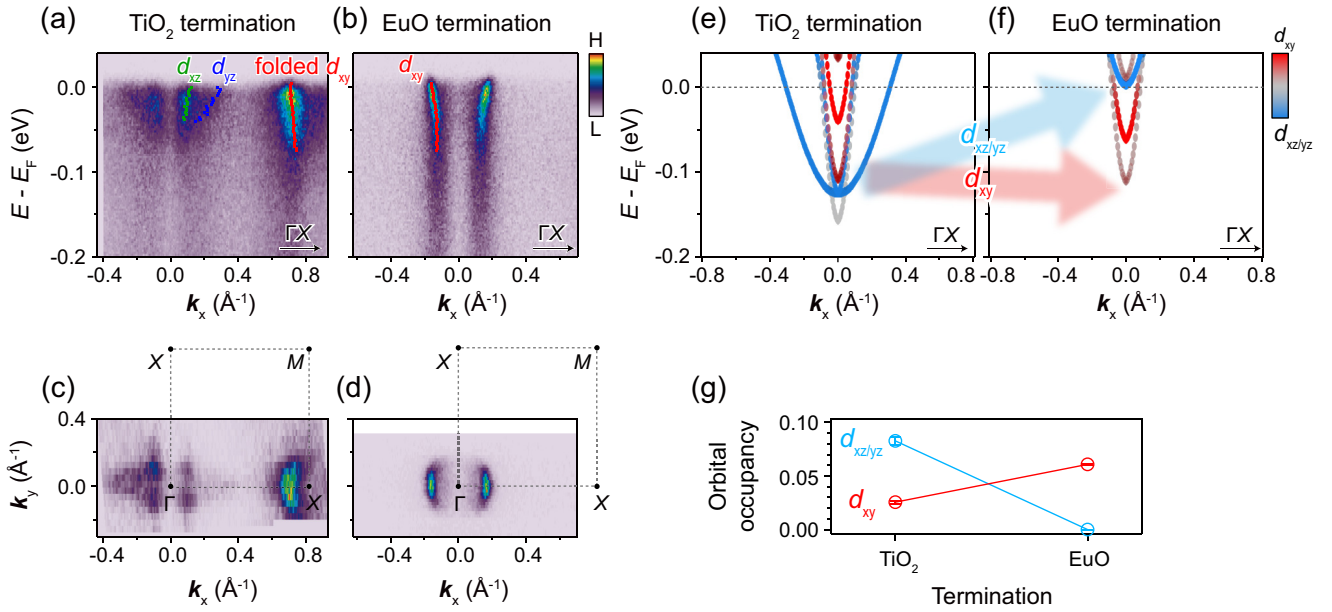

FIG. 3. Termination-dependent ETO 2DEG electronic structure. ARPES E-k cut along the high symmetric $\Gamma-X$ line for (a) TiO_2 termination and (b) EuO termination, respectively. Green, blue, and red dots represent the fit results with a Lorentzian function for d_{xz}, d_{yz}, and (2×2) folded d_{xy} bands, respectively. Note that the d_{xy} band in (a) is an electron band around the X point. Constant-energy ARPES map taken at E_F for (c) TiO_2 termination and (d) EuO termination, respectively. The black dashed line marks the quadrant of the Brillouin zone. Calculated band dispersions along the high symmetric $\Gamma-X$ line for (e) TiO_2 termination and (f) EuO termination, respectively. The E_F in calculation results was shifted by +350 meV for comparison with ARPES results, as noted in Fig. 2(c). (g) t_{2g} orbital occupancies for each termination, determined from the ARPES data analysis; see main text for the method.

In contrast, only the d_{xy} band is observed in the EuO-terminated ETO. This observation is consistent with the energy hierarchy of the t_{2g} orbitals predicted by DFT. If the energy levels of the d_{xz} and d_{yz} orbitals are raised above the E_F, it would explain why these bands are absent in the ARPES spectra of the EuO-terminated ETO.

We also quantitatively analyze the effect of termination conversion. Orbital occupancies were calculated by determining the ratio of pocket areas formed by each t_{2g} band to the total area of the first Brillouin zone [60,61]. For the quantitative analysis, we assume that the pockets formed by the $d_{xz/yz}$ bands are elliptical, while those formed by the d_{xy} band are circular [5]. The Fermi momenta (k_F) values needed to calculate the area of each band were extracted from high-symmetry lines in the ARPES results. For the TiO_2 termination, the values are 0.12, 0.28, and 0.10 for the d_{xz}, d_{yz}, and d_{xy} bands, respectively, whereas for the EuO termination, the d_{xy} value is 0.16. The termination-dependent orbital occupancy is shown in Fig. 3(g). At the EuO-terminated surface, the d_{xy} orbital dominates the 2DEG, while the $d_{xz/yz}$ orbitals dominate the 2DEG at the TiO_2-terminated surface. In other words, we experimentally demonstrate that the dominant orbital character of the 2DEG can be engineered through termination conversion.

Beyond orbital occupancy engineering, we investigate the effect of termination conversion on many-body interactions. In principle, when electrons couple with bosonic modes, the energy band dispersion undergoes renormalization, producing a so-called kink [60,62,63]. By analyzing the dispersion in ARPES spectra, we can determine both the energy scale of the coupled mode and the coupling strength. Figures 4(a) and 4(b) show the d_{xy} bands along the high-symmetry $\Gamma-X$ line for each termination. For EuO-terminated ETO, a kink feature is evident in the measured d_{xy} band, with an abrupt change in the slope of the band dispersion clearly observed near E_F—25 meV. In contrast, the d_{xy} band of the 2DEG at the TiO_2-terminated surface does not exhibit a clear kink feature.

Typically, the origin of the kink observed in ARPES is attributed to electron-phonon coupling. In this context, our observations can be associated with termination-dependent phonons or termination-dependent electron-phonon coupling. It is important to note that the elements and lattice constants are identical for both terminations. Given the nearly identical

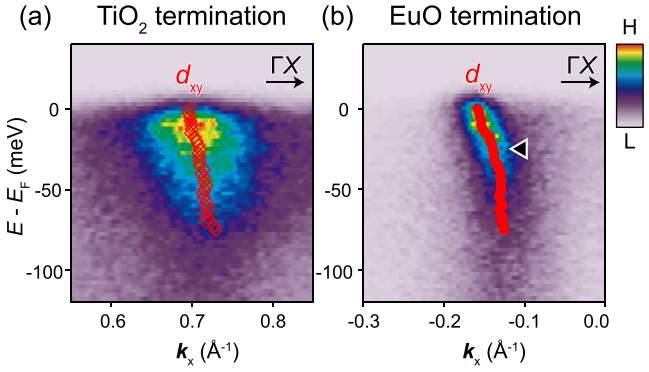

FIG. 4. Termination-dependent kink structure in ETO. E-k dispersion of (a) TiO_2-terminated and (b) EuO-terminated $EuTiO_3$ along the high symmetric $\Gamma-X$ line, with their Lorentzian fit result. In (b), black triangles highlight the kink position.

bulk structures, variations in bulk phonons are unlikely. Meanwhile, atomic displacements can occur at the surface where inversion symmetry is broken, and the magnitude or direction of these displacements can depend on the termination [64,65]. If these difference are large enough to impact the surface phonons, our observations may be attributed to surface phonon contributions.

On the other hand, considering the large magnetic moment of Eu^{2+}, a spin-related bosonic mode could also be a potential candidate for the origin of the kink [66,67]. Aforementioned surface atomic displacement can affect not only surface phonons, but also the hybridization of Eu and O states, which can mediate double-exchange-like interaction between Ti d_{xy} electrons [68]. Notably, a previous ARPES study reported the presence of a kink in a nonmagnetic 2DEG, while it was absent in a ferromagnetic 2DEG [28]. This suggests that spin-related bosonic modes, rather than phonons, could be responsible for the kink. In this scenario, the observed termination-dependent trend in the kink may indicate a termination-dependent magnetic transition in ETO. Moreover, the broader spectral feature observed in the TiO_2-terminated ETO may also suggest that ETO adopts different magnetic ground states depending on the termination. In ARPES, spectral broadening reflects an increased scattering rate (i.e., shorter quasiparticle lifetimes), which is known to occur near the Curie temperature in ferromagnets due to enhanced spin fluctuations [69]. Since the reported Curie temperature of ferromagnetic ETO is very low [34,47] and comparable to the temperature (10 K) at which our ARPES measurements were performed, the relatively broad spectrum in the TiO_2-terminated ETO may indicate a ferromagnetic ground state. Further studies, including direct magnetic measurements, are needed to clarify this behavior.

In summary, we engineered the termination of ETO by inserting an SRO layer and investigated its effect on the electronic structure of the 2DEG. First, we observed a termination-dependent change in the dominant orbital character of the 2DEG, which was further supported by our DFT calculations. Second, we found that the kink structure also varies with termination. The origin of this trend may be attributed to termination-dependent phonons or a termination-dependent magnetic transition, though further studies are needed to confirm this. Our results demonstrate that the design of oxide atomic terminations provides a viable pathway for realizing 2DEGs with engineered electronic properties.

ChatGPT was used to aid authors correct text to the use of definite/indefinite articles. We thank Younsik Kim for fruitful discussion. We are also grateful for support by the National Supercomputing Center with supercomputing resources (KSC-2025-CRE-0016) and computational resource of the UNIST Supercomputing center. This work was supported by the NRF funded by the Ministry of Science and ICT(RS-2023-00281839, RS-2024-00451261, RS-2023-00258359, RS-2024-00449996, RS-2024-00355333, NRF-2022R1A3B1077234), and by the National Research Council of Science and Technology(RS-2024-00410027). This work was also supported by the Institute of Applied Physics, Seoul National University.

Data availability. The data that support the findings of this article are openly available [70].

[1] H. Y. Hwang, Y. Iwasa, M. Kawasaki, B. Keimer, N. Nagaosa, and Y. Tokura, Emergent phenomena at oxide interfaces, Nat. Mater. **11**, 103 (2012).

[2] P. Yu, Y.-H. Chu, and R. Ramesh, Oxide interfaces: Pathways to novel phenomena, Mater. Today **15**, 320 (2012).

[3] F. Hellman, A. Hoffmann, Y. Tserkovnyak, G. S. Beach, E. E. Fullerton, C. Leighton, A. H. MacDonald, D. C. Ralph, D. A. Arena, H. A. Dürr, P. Fischer, J. Grollier, J. P. Heremans, T. Jungwirth, A. V. Kimel, B. Koopmans, I. N. Krivorotov, S. J. May, A. K. Petford-Long, J. M. Rondinelli, *et al.*, Interface-induced phenomena in magnetism, Rev. Mod. Phys. **89**, 025006 (2017).

[4] A. Ohtomo and H. Y. Hwang, A high-mobility electron gas at the $LaAlO_3/SrTiO_3$ heterointerface, Nature (London) **427**, 423 (2004).

[5] A. F. Santander-Syro, O. Copie, T. Kondo, F. Fortuna, S. Pailhès, R. Weht, X. G. Qiu, F. Bertran, A. Nicolaou, A. Taleb-Ibrahimi, P. Le Fèvre, G. Herranz, M. Bibes, N. Reyren, Y. Apertet, P. Lecoeur, A. Barthélémy, and M. J. Rozenberg, Two-dimensional electron gas with universal subbands at the surface of $SrTiO_3$, Nature (London) **469**, 189 (2011).

[6] W. Meevasana, P. D. C. King, R. H. He, S.-K. Mo, M. Hashimoto, A. Tamai, P. Songsiriritthigul, F. Baumberger, and Z.-X. Shen, Creation and control of a two-dimensional electron liquid at the bare $SrTiO_3$ surface, Nat. Mater. **10**, 114 (2011).

[7] Y. Matsubara, K. S. Takahashi, M. S. Bahramy, Y. Kozuka, D. Maryenko, J. Falson, A. Tsukazaki, Y. Tokura, and M. Kawasaki, Observation of the quantum Hall effect in δ-doped $SrTiO_3$, Nat. Commun. **7**, 11631 (2016).

[8] S. Gariglio, N. Reyren, A. D. Caviglia, and J.-M. Triscone, Superconductivity at the $LaAlO_3/SrTiO_3$ interface, J. Phys.: Condens. Matter **21**, 164213 (2009).

[9] J. Biscaras, N. Bergeal, A. Kushwaha, T. Wolf, A. Rastogi, R. C. Budhani, and J. Lesueur, Two-dimensional superconductivity at a Mott insulator/band insulator interface $LaTiO_3/SrTiO_3$, Nat. Commun. **1**, 89 (2010).

[10] J.-S. Lee, Y. W. Xie, H. K. Sato, C. Bell, Y. Hikita, H. Y. Hwang, and C.-C. Kao, Titanium d_{xy} ferromagnetism at the $LaAlO_3/SrTiO_3$ interface, Nat. Mater. **12**, 703 (2013).

[11] P. Moetakef, J. R. Williams, D. G. Ouellette, A. P. Kajdos, D. Goldhaber-Gordon, S. J. Allen, and S. Stemmer, Carrier-controlled ferromagnetism in $SrTiO_3$, Phys. Rev. X **2**, 021014 (2012).

[12] R. Di Capua, M. Verma, M. Radovic, V. N. Strocov, C. Piamonteze, E. B. Guedes, N. C. Plumb, Y. Chen, M. D'antuono, and G. M. De Luca, Orbital selective switching of ferromagnetism in an oxide quasi two-dimensional electron gas, npj Quantum Mater. **7**, 41 (2022).

[13] G. M. De Luca, R. Di Capua, E. Di Gennaro, F. M. Granozio, D. Stornaiuolo, M. Salluzzo, A. Gadaleta, I. Pallecchi, D.

Marrè, and C. Piamonteze, Transport properties of a quasi-two-dimensional electron system formed in $LaAlO_3/EuTiO_3/SrTiO_3$ heterostructures, Phys. Rev. B **89**, 224413 (2014).

[14] D. Stornaiuolo, C. Cantoni, G. M. De Luca, R. Di Capua, E. Di. Gennaro, G. Ghiringhelli, B. Jouault, D. Marrè, D. Massarotti, and F. Miletto Granozio, Tunable spin polarization and superconductivity in engineered oxide interfaces, Nat. Mater. **15**, 278 (2016).

[15] A. D. Caviglia, M. Gabay, S. Gariglio, N. Reyren, C. Cancellieri, and J.-M. Triscone, Tunable Rashba spin-orbit interaction at oxide interfaces, Phys. Rev. Lett. **104**, 126803 (2010).

[16] E. Lesne, Y. Fu, S. Oyarzun, J. C. Rojas-Sánchez, D. C. Vaz, H. Naganuma, G. Sicoli, J.-P. Attané, M. Jamet, E. Jacquet, J.-M. George, A. Barthélémy, H. Jaffrès, A. Fert, M. Bibes, and L. Vila, Highly efficient and tunable spin-to-charge conversion through Rashba coupling at oxide interfaces, Nat. Mater. **15**, 1261 (2016).

[17] H. Xu, H. Li, N. Gauquelin, X. Chen, W.-F. Wu, Y. Zhao, L. Si, D. Tian, L. Li, Y. Gan, S. Qi, M. Li, F. Hu, J. Sun, D. Jannis, P. Yu, G. Chen, Z. Zhong, M. Radovic, J. Verbeeck, *et al.*, Giant tunability of Rashba splitting at cation-exchanged polar oxide interfaces by selective orbital hybridization, Adv. Mater. **36**, 2313297 (2024).

[18] L. M. Vicente-Arche, J. Bréhin, S. Varotto, M. Cosset-Cheneau, S. Mallik, R. Salazar, P. Noël, D. C. Vaz, F. Trier, S. Bhattacharya, A. Sander, P. Le Fèvre, F. Bertran, G. Saiz, G. Ménard, N. Bergeal, A. Barthélémy, H. Li, C.-C. Lin, D. E. Nikonov, *et al.*, Spin-charge interconversion in $KTaO_3$ 2D electron gases, Adv. Mater. **33**, 2102102 (2021).

[19] A. Gupta, H. Silotia, A. Kumari, M. Dumen, S. Goyal, R. Tomar, N. Wadehra, P. Ayyub, and S. Chakraverty, $KTaO_3$-The new kid on the spintronics block, Adv. Mater. **34**, 2106481 (2022).

[20] H. Zhang, H. Zhang, X. Yan, X. Zhang, Q. Zhang, J. Zhang, F. Han, L. Gu, B. Liu, Y. Chen, B. Shen, and J. Sun, Highly mobile two-dimensional electron gases with a strong gating effect at the amorphous $LaAlO_3/KTaO_3$ interface, ACS Appl. Mater. Interfaces **9**, 36456 (2017).

[21] K. S. Im, J. B. Ha, K. W. Kim, J. S. Lee, D. S. Kim, S. H. Hahm, and J. H. Lee, Normally off GaN MOSFET based on AlGaN/GaN heterostructure with extremely high 2DEG density grown on silicon substrate, IEEE Electron Device Lett. **31**, 192 (2010).

[22] S. N. Rebec, T. Jia, H. M. Sohail, M. Hashimoto, D. Lu, Z.-X. Shen, and R. G. Moore, Dichotomy of the photo-induced 2-dimensional electron gas on $SrTiO_3$ surface terminations, Proc. Natl. Acad. Sci. USA **116**, 16687 (2019).

[23] S. Muff, M. Fanciulli, A. P. Weber, N. Pilet, Z. Ristić, Z. Wang, N. C. Plumb, M. Radović, and J. H. Dil, Observation of a two-dimensional electron gas at $CaTiO_3$ film surfaces, Appl. Surf. Sci. **432**, 41 (2018).

[24] E. N. Jin, L. Kornblum, D. P. Kumah, K. Zou, C. C. Broadbridge, J. H. Ngai, C. H. Ahn, and F. J. Walker, A high density two-dimensional electron gas in an oxide heterostructure on Si (001), APL Mater. **2**, 116109 (2014).

[25] M. Bianchi, D. Guan, S. Bao, J. Mi, B. B. Iversen, P. D. C. King, and P. Hofmann, Coexistence of the topological state and a two-dimensional electron gas on the surface of Bi_2Se_3, Nat. Commun. **1**, 128 (2010).

[26] B. Sohn, G. Marcaud, Y. Shin, S. Lee, T. Werner, T. Yilmaz, J. Yang, W. Wei, A. Fedorov, E. Vescovo, Y. He, S. Ismail-Beigi, C. H. Ahn, and F. J. Walker, Observation of orbital selective charge transfer in a $Fe/BaTiO_3$ interfacial two-dimensional electron gas, Phys. Rev. B **109**, 155106 (2024).

[27] H. Zhang, Y. Yun, X. Zhang, H. Zhang, Y. Ma, X. Yan, F. Wang, G. Li, R. Li, T. Khan, Y. Chen, W. Liu, F. Hu, B. Liu, B. Shen, W. Han, and J. Sun, High-mobility spin-polarized two-dimensional electron gases at $EuO/KTaO_3$ interfaces, Phys. Rev. Lett. **121**, 116803 (2018).

[28] P. Lömker, T. C. Rödel, T. Gerber, F. Fortuna, E. Frantzeskakis, P. Le Fèvre, F. Bertran, M. Müller, and A. F. Santander-Syro, Two-dimensional electron system at the magnetically tunable $EuO/SrTiO_3$ interface, Phys. Rev. Mater. **1**, 062001 (2017).

[29] H. Zhang, Y. Ma, H. Zhang, X. Chen, S. Wang, G. Li, Y. Yun, X. Yan, Y. Chen, F. Hu, J. Cai, B. Shen, W. Han, and J. Sun, Thermal spin injection and inverse Edelstein effect of the two-dimensional electron gas at $EuO-KTaO_3$ interfaces, Nano Lett. **19**, 1605 (2019).

[30] P. R. Hammar, B. R. Bennett, M. J. Yang, and M. Johnson, Observation of spin injection at a ferromagnet-semiconductor interface, Phys. Rev. Lett. **83**, 203 (1999).

[31] H. Shin, C. Liu, S. Godin, F. Li, R. Sutarto, B. A. Davidson, and K. Zou, Highly tunable ferromagnetic 2D electron gases at oxide interfaces, Adv. Mater. Interf. **9**, 2201475 (2022).

[32] R. Di Capua, M. Verma, M. Radović, N. C. Plumb, J. H. Dil, Z. Ristić, E. B. Guedes, G. M. De Luca, D. Preziosi, Z. Wang, A. P. Weber, R. Pentcheva, and M. Salluzzo, Two-dimensional electron gas at the (001) surface of ferromagnetic $EuTiO_3$, Phys. Rev. Res. **3**, L042038 (2021).

[33] P. Wadhwa and A. Filippetti, Fully spin-polarized, two-dimensional hole and electron gases at the highly polar (111) $EuTiO_3/SrTiO_3$ interface, ACS Appl. Electron. Mater. **6**, 3657 (2024).

[34] D. Shin, I. Kim, S. Song, Y.-S. Seo, J. Hwang, S. Park, M. Choi, and W. S. Choi, Defect engineering of magnetic ground state in $EuTiO_3$ epitaxial thin films, J. Am. Ceram. Soc. **104**, 4606 (2021).

[35] H. Shin, C. Liu, F. Li, R. Sutarto, B. A. Davidson, and K. Zou, Controlling the electrical and magnetic ground states by doping in the complete phase diagram of titanate $Eu_{1-x}La_xTiO_3$ thin films, Phys. Rev. B **101**, 214105 (2020).

[36] T. R. McGuire, M. W. Shafer, R. J. Joenk, H. A. Alperin, and S. J. Pickart, Magnetic structure of $EuTiO_3$, J. Appl. Phys. **37**, 981 (1966).

[37] K. S. Takahashi, H. Ishizuka, T. Murata, Q. Y. Wang, Y. Tokura, N. Nagaosa, and M. Kawasaki, Anomalous Hall effect derived from multiple Weyl nodes in high-mobility $EuTiO_3$ films, Sci. Adv. **4**, eaar7880 (2018).

[38] K. Ahadi, H. Kim, and S. Stemmer, Spontaneous Hall effects in the electron system at the $SmTiO_3/EuTiO_3$ interface, APL Mater. **6**, 056102 (2018).

[39] K. S. Takahashi, M. Onoda, M. Kawasaki, N. Nagaosa, and Y. Tokura, Control of the anomalous Hall effect by doping in $Eu_{1-x}La_xTiO_3$ thin films, Phys. Rev. Lett. **103**, 057204 (2009).

[40] K. Ahadi, L. Galletti, and S. Stemmer, Evidence of a topological Hall effect in $Eu_{1-x}Sm_xTiO_3$, Appl. Phys. Lett. **111**, 172403 (2017).

[41] H. Yamada, A. Tsurumaki-Fukuchi, M. Kobayashi, T. Nagai, Y. Toyosaki, H. Kumigashira, and A. Sawa, Strong

surface-termination effect on electroresistance in ferroelectric tunnel junctions, Adv. Funct. Mater. **25**, 2708 (2015).

[42] W. Zhang, H. Y. Lu, D. H. Xie, W. Feng, S. Y. Tan, Y. Liu, X. G. Zhu, Y. Zhang, Q. Q. Hao, Y. B. Huang, X. C. Lai, and Q. Y. Chen, ARPES/STM study of the surface terminations and $5f$-electron character in URu_2Si_2, Phys. Rev. B **98**, 115121 (2018).

[43] Q. D. Gibson, L. M. Schoop, A. P. Weber, H. Ji, S. Nadj-Perge, I. K. Drozdov, H. Beidenkopf, J. T. Sadowski, A. Fedorov, A. Yazdani, T. Valla, and R. J. Cava, Termination-dependent topological surface states of the natural superlattice phase Bi_4Se_3, Phys. Rev. B **88**, 081108 (2013).

[44] Z.-L. Yu, Q.-R. Ma, Y.-Q. Zhao, B. Liu, and M.-Q. Cai, Surface termination-A key factor to influence electronic and optical properties of $CsSnI_3$, J. Phys. Chem. C **122**, 9275 (2018).

[45] M. S. Park, S. H. Rhim, and A. J. Freeman, Charge compensation and mixed valency in $LaAlO_3/SrTiO_3$ heterointerfaces studied by the FLAPW method, Phys. Rev. B **74**, 205416 (2006).

[46] D. P. Kumah, A. Malashevich, A. S. Disa, D. A. Arena, F. J. Walker, S. Ismail-Beigi, and C. H. Ahn, Effect of surface termination on the electronic properties of $LaNiO_3$ films, Phys. Rev. Appl. **2**, 054004 (2014).

[47] H. G. Lee, L. Wang, L. Si, X. He, D. G. Porter, J. R. Kim, E. K. Ko, J. Kim, S. M. Park, B. Kim, A. T. S. Wee, A. Bombardi, Z. Zhong, and T. W. Noh, Atomic-scale metal-insulator transition in $SrRuO_3$ ultrathin films triggered by surface termination conversion, Adv. Mater. **32**, 1905815 (2020).

[48] G. Rijnders, D. H. A. Blank, J. Choi, and C.-B. Eom, Enhanced surface diffusion through termination conversion during epitaxial $SrRuO_3$ growth, Appl. Phys. Lett. **84**, 505 (2004).

[49] See Supplemental Material at http://link.aps.org/supplemental/10.1103/dx5k-dwgv for experimental supplementary figures; methods; details on $SrRuO_3$-thickness-dependent $EuTiO_3/SrRuO_3/SrTiO_3$ surface 2DEG band structure; Surface characterization result using Low-energy electron diffraction and reflection high-energy electron diffraction; Termination-dependent constant-energy angle-resolved photoemission spectroscopy map taken at Fermi level by rotating azimuthal angle; Termination-dependent angle-integrated valence band spectra; Calculated density of Eu 4f states projected onto the top two $EuTiO_3$ layers for each termination; Characterization result using transmission electron microscopy. The Supplemental Material also contains Ref. [50].

[50] J. Xia, W. Siemons, G. Koster, M. R. Beasley, and A. Kapitulnik, Critical thickness for itinerant ferromagnetism in ultrathin films of $SrRuO_3$, Phys. Rev. B **79**, 140407 (2009).

[51] P. Giannozzi, S. Baroni, N. Bonini, M. Calandra, R. Car, C. Cavazzoni, D. Ceresoli, G. L. Chiarotti, M. Cococcioni, I. Dabo, A. D. Corso, S. de Gironcoli, S. Fabris, G. Fratesi, R. Gebauer, U. Gerstmann, C. Gougoussis, A. Kokalj, M. Lazzeri, L. Martin-Samos, *et al.*, QUANTUM ESPRESSO: A modular and open-source software project for quantum simulations of materials, J. Phys.: Condens. Matter **21**, 395502 (2009).

[52] P. Giannozzi Jr, O. Andreussi, T. Brumme, O. Bunau, M. B. Nardelli, M. Calandra, R. Car, C. Cavazzoni, D. Ceresoli, M. Cococcioni, N. Colonna, I. Carnimeo, A. D. Corso, S. de Gironcoli, P. Delugas, R. A. DiStasio, A. Ferretti, A. Floris, G. Fratesi, G. Fugallo, *et al.*, Advanced capabilities for materials modeling with QUANTUM ESPRESSO, J. Phys.: Condens. Matter **29**, 465901 (2017).

[53] G. Prandini, A. Marrazzo, I. E. Castelli, N. Mounet, and N. Marzari, Precision and efficiency in solid-state pseudopotential calculations, npj Comput. Mater. **4**, 72 (2018).

[54] K. F. Garrity, J. W. Bennett, K. M. Rabe, and D. Vanderbilt, Pseudopotentials for high-throughput DFT calculations, Comput. Mater. Sci. **81**, 446 (2014).

[55] E. Küçükbenli, M. Monni, B. I. Adetunji, X. Ge, G. A. Adebayo, N. Marzari, S. de Gironcoli, and A. D. Corso, Projector augmented-wave and all-electron calculations across the periodic table: A comparison of structural and energetic properties, arXiv:1404.3015.

[56] M. Topsakal and R. M. Wentzcovitch, Accurate projected augmented wave (PAW) datasets for rare-earth elements (RE = La−Lu), Comput. Mater. Sci. **95**, 263 (2014).

[57] S. L. Dudarev, G. A. Botton, S. Y. Savrasov, C. J. Humphreys, and A. P. Sutton, Electron-energy-loss spectra and the structural stability of nickel oxide: An LSDA+U study, Phys. Rev. B **57**, 1505 (1998).

[58] Y.-L. Huang, H.-J. Liu, C.-H. Ma, P. Yu, Y.-H. Chu, and J.-C. Yang, Pulsed laser deposition of complex oxide heteroepitaxy, Chin. J. Phys. **60**, 481 (2019).

[59] P. Schütz, M. Kamp, D. Di Sante, A. Lubk, B. Büchner, G. Sangiovanni, M. Sing, and R. Claessen, Electronic structure of epitaxial perovskite films in the two-dimensional limit: Role of the surface termination, Appl. Phys. Lett. **116**, 201601 (2020).

[60] A. Damascelli, Z. Hussain, and Z.-X. Shen, Angle-resolved photoemission studies of the cuprate superconductors, Rev. Mod. Phys. **75**, 473 (2003).

[61] J. M. Luttinger, Fermi surface and some simple equilibrium properties of a system of interacting fermions, Phys. Rev. **119**, 1153 (1960).

[62] J. A. Sobota, Y. He, and Z.-X. Shen, Angle-resolved photoemission studies of quantum materials, Rev. Mod. Phys. **93**, 025006 (2021).

[63] P. Hofmann, I. Y. Sklyadneva, E. D. L. Rienks, and E. V. Chulkov, Electron–phonon coupling at surfaces and interfaces, New J. Phys. **11**, 125005 (2009).

[64] Z.-Q. Li, J.-L. Zhu, C. Q. Wu, Z. Tang, and Y. Kawazoe, Relaxations of TiO_2- and SrO-terminated $SrTiO_3$ (001) surfaces, Phys. Rev. B **58**, 8075 (1998).

[65] J. Padilla and D. Vanderbilt, *Ab initio* study of $BaTiO_3$ surfaces, Phys. Rev. B **56**, 1625 (1997).

[66] T. L. Yu, M. Xu, W. T. Yang, Y. H. Song, C. H. P. Wen, Q. Yao, X. Lou, T. Zhang, W. Li, X. Y. Wei, J. K. Bao, G. H. Cao, P. Dudin, J. D. Denlinger, V. N. Strocov, R. Peng, H. C. Xu, and D. L. Feng, Strong band renormalization and emergent ferromagnetism induced by electron-antiferromagnetic-magnon coupling, Nat. Commun. **13**, 6560 (2022).

[67] P. Li, Y. Wang, Y. Liu, J. Yao, Z. Zhao, Z. Liu, D. Shen, H. Luo, G. Cao, J. Jiang, and D. Feng, Revealing the electron-spin fluctuation coupling by photoemission in $CaKFe_4As_4$, Phys. Rev. X **15**, 021001 (2025).

[68] D. Odkhuu, S. H. Rhim, D. Shin, and N. Park, La displacement driven double-exchange like mediation in titanium d_{xy}

ferromagnetism at the $LaAlO_3/SrTiO_3$, J. Phys. Soc. Jpn. **85**, 043702 (2016).

[69] S. Hahn, B. Sohn, M. Kim, J. R. Kim, S. Huh, Y. Kim, W. Kyung, M. Kim, D. Kim, Y. Kim, T. W. Noh, J. H. Shim, and C. Kim, Observation of spin-dependent dual ferromagnetism in perovskite ruthenates, Phys. Rev. Lett. **127**, 256401 (2021).

[70] S. Hahn, Dataset for "Termination-dependent electronic structure of $EuTiO_3$ surface 2DEG", Zenodo (2025), doi:10.5281/zenodo.16644262.